Intraseasonal sea level variability along the western coast of India simulated by an eddy-resolving ocean general circulation model

Yoko Yamagami[1], Tatsuo Suzuki[1], and Hiroaki Tatebe[2]

[1]Japan Agency for Marine-Earth Science and Technology
[2]JAMSTEC

February 26, 2024

Abstract

Future sea level rise under global warming poses serious risks of extreme sea level events in coastal regions worldwide. Numerous state-of-the-art climate models, with their relatively coarse horizontal resolution, may not adequately resolve coastal wave dynamics, leading to uncertainties in coastal sea level variability representation. This study compared eddy-resolving and non-eddying ocean models in reproducing sea level variability, focusing on the probability distribution along the western coast of India. The eddy-resolving model can simulate intraseasonal sea level variations associated with coastal waves driven by equatorial wind anomalies. The non-eddying model fails to capture over 81% of observed extreme sea level events, as shown in the probability distribution for intraseasonal time series. Although capable of simulating Indian Ocean Dipole-related low-frequency sea level anomalies, the non-eddying model does not replicate their connection to intraseasonal extreme events. The results suggest that climate model projections may underestimate future changes in extreme sea level events.

Hosted file

main_YST2024.docx available at https://authorea.com/users/745264/articles/717413-intraseasonal-sea-level-variability-along-the-western-coast-of-india-simulated-by-an-eddy-resolving-ocean-general-circulation-model

Intraseasonal sea level variability along the western coast of India simulated by an eddy-resolving ocean general circulation model

Y. Yamagami[1], T. Suzuki[1], H. Tatebe[1]

[1] Japan Agency for Marine-Earth Science and Technology, Yokohama, Japan

Corresponding author: Yoko Yamagami (y.yamagami@jamstec.go.jp)

† Research Center for Environmental Modeling and Application, Japan Agency for Marine-Earth Science and Technology, 3173-25 Showamachi, Kanazawaku, Yokohama, Kanagawa 236-0001, Japan

Key Points:

- Reproducibility of sea level variability is compared along the western coast of India using eddy-resolving and non-eddying ocean models.
- The eddy-resolving model captures coastal Kelvin waves arising from Indian Ocean dipole and consequent intraseasonal sea level variations.
- The non-eddying model may miss over 81% of the extreme sea level events compared to observations.

Abstract

Future sea level rise under global warming poses serious risks of extreme sea level events in coastal regions worldwide. Numerous state-of-the-art climate models, with their relatively coarse horizontal resolution, may not adequately resolve coastal wave dynamics, leading to uncertainties in coastal sea level variability representation. This study compared eddy-resolving and non-eddying ocean models in reproducing sea level variability, focusing on the probability distribution along the western coast of India. The eddy-resolving model can simulate intraseasonal sea level variations associated with coastal waves driven by equatorial wind anomalies. The non-eddying model fails to capture over 81% of observed extreme sea level events, as shown in the probability distribution for intraseasonal time series. Although capable of simulating Indian Ocean Dipole-related low-frequency sea level anomalies, the non-eddying model does not replicate their connection to intraseasonal extreme events. The results suggest that climate model projections may underestimate future changes in extreme sea level events.

Plain Language Summary

Sea level variations in the northern Indian Ocean are influenced by ocean waves near the coast, typically in a horizontal scale of approximately 100 km. It is not clear if these coastal waves and their movement are accurate represented in climate simulations, which typically have a relatively coarse horizontal resolution. This study compared sea level variations along the western coast of India using two ocean models with coarse and fine horizontal resolutions. We found that the high-resolution model adequately simulates the generation and propagation of coastal waves, and thus successfully simulate sea level variations with a 20–150-day time scale along western India. This result suggests that many recent climate simulations may have underestimated the frequency of extreme sea level events in coastal regions.

1 Introduction

Global warming is projected to cause persistent sea level rise worldwide (IPCC 2022a). In addition to the global mean sea level rise owing to thermal expansion, melting of glaciers, etc., extreme sea level projections associated with changes in atmospheric circulation and river runoff are also required in coastal regions, especially projections of changes in the occurrence of extreme events (IPCC 2022b). Given that many of the state-of-art climate models in the Coupled Model Intercomparison Project Phase 6 (CMIP6) use a relatively coarse horizontal resolution of approximately 100 km, the projections obtained using these models may underestimate influence of oceanic mesoscale structures and coastal phenomena. Hence, it remains unclear whether current sea level projections, particularly in coastal regions, adequately capture changes in extreme sea level events (i.e., as indicated by the tails in probability distributions).

In the densely populated coastal areas of the northern Indian Ocean, projected sea level rises in the Arabian Sea and the Bay of Bengal (Han et al., 2010; Jyoti et al., 2023) present serious risks, including coastal storm surges and extreme tidal events. Sea level variability along the coasts of the northern Indian Ocean is strongly influenced by equatorial waves and their resultant coastal Kelvin wave. Clarke and Liu (1994) showed that the interannual sea level anomalies (SLA) along the coasts of the northern Indian Ocean were remotely triggered by equatorial zonal winds. More recently, using linear stratified models (McCreary, 1996), several studies have investigated how wind stress forcing over the Arabian Sea, the southern tip of Sri Lanka, and the equatorial Indian Ocean impacts intraseasonal-to-interannual sea level variations along the coast of India (Suresh et al., 2013, 2016, 2018). Wind variations leading to coastal Kelvin waves can be attributed to semiannual basin-scale wind variability that drives the equatorial jet (Yoshida, 1959; Wyrtki, 1973), intraseasonal anomalies associated with the Madden-Julian Oscillation (MJO; Madden & Julian, 1977), and interannual anomalies associated with the Indian Ocean Dipole (IOD) (Saji et al., 1999; Han & Webster, 2002; Aparna et al., 2012).

Although previous studies suggested the potential role of coastal Kelvin waves in the Northern Indian Ocean, the extent to which standard climate models reproduce the coastal sea level variations remains unclear. Therefore, using the coastal sea level variability along western India as an illustrative example, this study undertakes a comparative analysis of multiple simulations derived from the oceanic component utilized in a climate model. Here we show that an eddy-resolving ocean general circulation model (OGCM) is required to accurately represent sea level variations along the western coast of India. In particular, since intraseasonal sea level variations have a relatively pronounced amplitude and consequently lead to extreme events, this study focuses mainly on how the intraseasonal variations in coastal sea level are represented in OGCMs. Even though the non-eddying OGCM simulation is forced by the same atmospheric boundary conditions as in the eddy-resolving OGCM, the coarse horizontal resolution of the non-eddying OGCM fails to accurately capture the sea level variability, especially variations originating from the equator through the coastal wave guide in the Bay of Bengal.

2 Models, Data, and Methods

This study compares two simulations of CCSR Ocean Component Model (COCO) (Hasumi, 2006), which serves as the sea ice-ocean component of the sixth version of the Model for Interdisciplinary Research on Climate (MIROC6; Tatebe et al., 2019) that was developed cooperatively by the Japanese climate modeling community. The configurations of the coarse stand-alone OGCM used in the present study are exactly the same as the global OGCM component of MIROC6. The model employs a nominal 1° horizontal resolution in a tripolar coordinate system, and there are 63 vertical levels, including the lowermost layer that incorporates bottom boundary layer parameterization (Nakano & Suginohara, 2002). This simulation is referred to as “COCO-LR” hereafter. We also used a global high-resolution version of COCO, which has horizontal resolution of 0.1° (hereafter referred to as COCO-HR). Using the phase 2 protocol of the Ocean Model Intercomparison Project (OMIP2; Tsujino et al., 2020), an endorsed Multi-Model Intercomparison Project (MIP) of CMIP6, both models were initialized using observed temperature and salinity data from the World Ocean Atlas 2013 version 2 (Locarnini et al., 2013; Zweng et al., 2013). The models were driven by JRA55-do 3-hourly surface forcings (Tsujino et al., 2020) from 1958 to 2019 for COCO-HR and to 2018 for COCO-LR (Komuro, 2019). In the COCO-HR model, regardless of the existence of sea ice, sea surface salinity (SSS) above the latitudes of 60°N and below 60°S was weakly relaxed to observational data with a 10-day restoring timescale to avoid model drift. Similarly, temperature and salinity at depths greater than 1500 m were also restored to observed values with a 5-year timescale. Note that COCO-HR improved the representation of the mean state in the Indian Ocean (see Text S1 for details).

To highlight the impact of interannual variations in surface wind forcing on the coastal sea level along the western coast of India, we also conducted a sensitivity experiment, hereafter referred to as “WIND0”. In this experiment, we used only the 3-hourly climatological mean of surface wind data for calculating surface wind stresses in COCO-HR. Thus, the surface wind stresses (i.e., dynamical forcing) in WIND0 incorporate only climatological mean variations, excluding low-frequency variations that occur over periods longer than 1 year. Other surface forcings in WIND0, such as surface heat flux, freshwater flux, and river runoff (i.e., thermodynamical forcing), are the same as those in COCO-HR.

In this study, we used the following observational datasets. PCMDI-SST (Hurrell et al., 2008) was used for the monthly sea surface temperature (SST) data for the period 1993–2019 with a horizontal resolution 1°×1°, as in Tsujino et al. (2020). CMEMS sea level products (DUACS DT2014; Pujol et al., 2016) have a daily interval and a horizontal resolution of 0.25°×0.25° for the period 1993–2019. Drifter-derived monthly climatological surface currents data were also used (Laurindo et al., 2017). To compare sea level anomalies with the satellite altimeter products, we mainly analyzed model outputs after 1993.

To examine SLA propagation in the coastal area, we calculated lag composites of SLA for extreme sea level events. A two-tailed *t*-test was adapted to the statistical test at 90% confidence level. To estimate the probability density functions (PDFs) of SLA, Kernel Density estimation was applied (Dehand, 1987; Marshall & Molteni, 1993). A Butterworth filter was employed to isolate the intraseasonal variability within the 20-150 day period.

3 Sea level variance in the Northern Indian Ocean

In this section, we briefly validate the COCO-HR model focusing on sea level variability. COCO-HR showed noticeable improvements in the northern Indian Ocean, especially in regions where oceanic mesoscale eddies are dominant (Fig. 1). Regarding seasonal variability, observational data showed large-amplitude sea level variance in the Arabian Sea and the Bay of Bengal (Fig. 1a). These patterns are explained by the seasonal dynamics of the Lakshadweep High/Low in the southern Arabian Sea (Vinayachandran et al., 2007) and coastal wave guide effect in the Bay of Bengal (Clarke & Liu, 1994). The general structure of this seasonal sea level variability is well represented in the COCO-HR model, both in terms of spatial pattern and amplitude (Fig. 1b). Although the COCO-LR model showed a similar pattern, the overall amplitude was smaller than that in COCO-HR (Fig. 1c), suggesting that the coarse resolution model underestimates the seasonal sea level variability in the northern Indian Ocean.

In addition, COCO-HR more accurately captures detrended interannual SLAs compared to COCO-LR (Fig. 1d-f). The noticeable interannual variations in the Somalia-Oman upwelling region are well represented in COCO-HR, aligning closely with observations, although COCO-

HR does slightly underestimate them. This difference is presumably because the interannual variability of the mesoscale variability associated with the Somali Current is well represented in COCO-HR. Interannual sea level variability in the western Bay of Bengal also tends to be better represented in COCO-HR, indicating that the interannual variability of coastal trapped waves and local mesoscale variability is also well captured by COCO-HR. In the following section, we examined sea level variations along the western coast of India in greater detail.

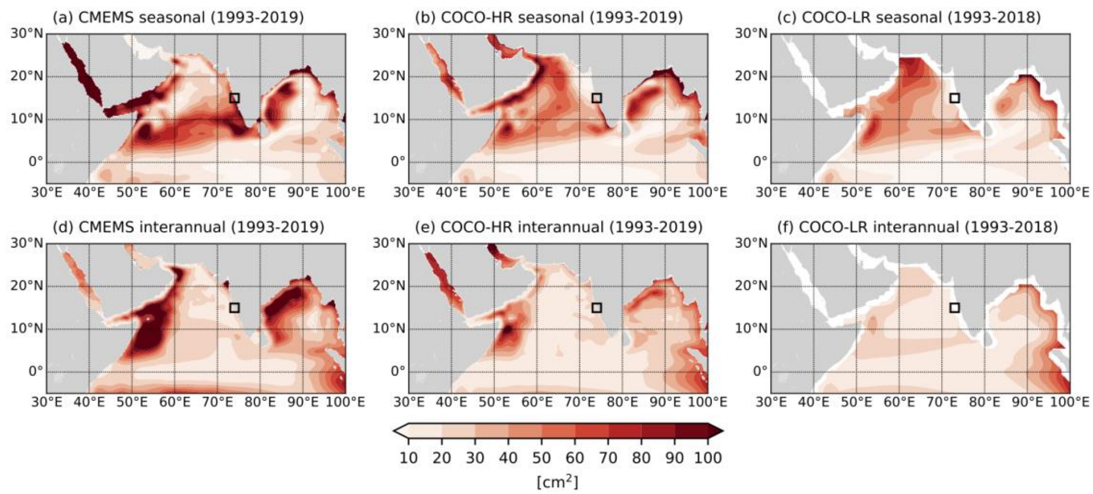

Figure 1. Variances in seasonal sea level anomalies (SLAs) [cm^2] in the northern Indian Ocean for (a) observations, (b) COCO-HR, and (c) COCO-LR. (d)-(f) As in (a)-(c), but for interannual SLAs. Interannual anomalies are defined as detrended anomalies from the climatology.

4 SLAs along the western coast of India

4.1 Intraseasonal sea level variations

In order to investigate sea level variations along the western coast of India, area-averaged sea level variations are calculated within 2°×2° boxes at 15°N (black boxes in Fig. 1). Note that qualitatively similar results are obtained if we use 1°×1° boxes. The comparison indicates that COCO-HR more accurately represents both seasonal (Text S2) and intraseasonal SSH variations along the west coast of India.

PDFs for 20-150 day band-passed SLA time series are estimated (Fig. 2). Note that we refer to the 20-150 day band-passed timeseries of detrended anomalies from the daily climatology as “intraseasonal anomalies” hereafter. In all months, COCO-HR reproduces PDFs that are similar to the observational data, with standard deviations that also match those of the observational data. Conversely, COCO-LR exhibits smaller standard deviations for each PDF compared to the observations, resulting in underestimation of extreme SLA events. Indeed, in the observational data, the thresholds employed for positive (negative) extreme SLA events, i.e., events exceeding 95% (5.0%) probability, are estimated to be 4.4 cm (-4.8 cm) (Fig. 2a). For COCO-HR, the occurrence rates of positive (negative) extreme SLA events are 7.3% (4.7%), which is consistent with the observed rates. For COCO-LR, the occurrence of positive (negative) SLA events is 0.95% (0.21%), which is considerably smaller than in the observations. This result means that COCO-LR misses 81% (96%) of the extreme intraseasonal sea level maxima (minima), and underscores the importance of using an eddy-resolving ocean model to accurately hindcast coastal sea level variability.

The narrower PDFs (i.e., indicating less variance) in WIND0 compared to COCO-HR suggests a reduced occurrence of extreme SLA events. Therefore, dynamical wind forcing anomalies are necessary for simulating intraseasonal SLA along the western coast of India (Fig. 2b-m). This result also implies that the contribution of factors other than wind stress forcing, such as buoyancy flux and baroclinic instability associated with West Indian Coastal Current (e.g., Varna et al., 2023), is not predominant. The above result remains qualitatively unchanged if the PDFs are calculated for detrended anomalies without 20–150-day bandpass filtering (Fig. S5). Thus, differences in anomalies with periods shorter (longer) than 20 (150) days do not explain the reduction in the standard deviation of PDFs in WIND0. Consequently, the higher frequency of extreme SLA events in COCO-HR can be attributed to interannual-to-decadal changes in the intraseasonal amnomalies. Given that the variance in the intraseasonal component is prominent in both the observation and models (Fig. S6), compared to the total variance, we will discuss the processes driving these differences in PDFs of intraseasonal variability in the next section.

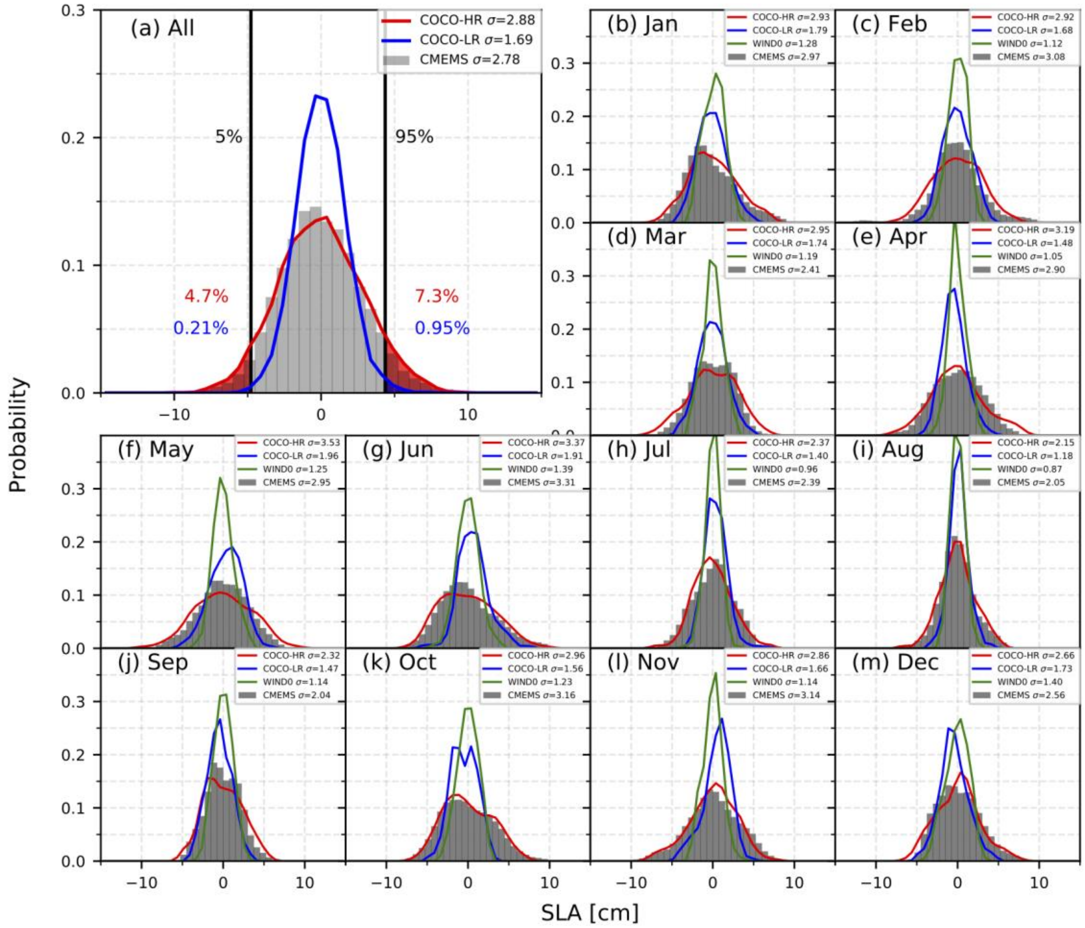

Figure 2. Probability density functions (PDFs) of intraseasonal (20-150 days) sea level anomalies (SLA) [cm] along the western coast of India (15°N) for observations (CMEMS; black bars), COCO-HR (red lines), COCO LR (blue lines), and WIND0 (green lines) for (a) all seasons and (b)-(m) each month. PDFs are estimated by kernel density estimation. The standard deviation (σ) for each month is given in the legend accompanying each graph. All PDFs are normalized and the vertical axis indicates probability (unit less). In (a), vertical black lines indicate the 5% and 95% anomalies based on CMEMS data. Areas where anomalies exceed the 5 or 95 percentiles for CMEMS are highlighted in red (COCO-HR) and blue (COCO-LR) colors, respectively, with the corresponding percentile values marked in each model.

4.2 Resolution dependency of the propagation of coastal Kelvin waves

Regarding the remote impacts of coastal Kelvin waves on the western coast of India, the large intraseasonal SLA variances in COCO-HR may be attributed to the propagation of sea level anomalies. Figure 3 shows a lag composite of SLA from 0 to 40 days before the occurrence of intraseasonal SLA exceeds +1 standard deviation at the western coast of India (indicated by red symbols in Fig. S6). Since the composites obtained for the negative anomalies are almost mirror images, we discuss only the results obtained for positive SLA events. In the observations, a significant SLA associated with equatorial Kelvin wave is triggered by westerly wind anomalies in the tropical Indian Ocean 40 days prior. Subsequently, this wave reaches the coast of Sumatra island and then propagates as coastal Kelvin waves along the coast of the Bay of Bengal. These waves pass through the southern tip of India, arrive at the western coast of India, and eventually extend into the northern Arabian Sea (Fig. 3a). Furthermore, SLAs also appear to be radiated from the eastern coast of the Bay of Bengal as westward Rossby waves, and are enhanced by easterly wind anomalies along the southern tip of Sri Lanka.

In COCO-HR, similar to the observations, the equatorial Kelvin wave enters the eastern boundary and propagates as coastal Kelvin waves from the Bay of Bengal to the western coast of India (Fig. 3b). Westward SLAs also appeared to be radiated from the eastern coast of the Bay of Bengal to the southern coast of India. On the other hand, COCO-LR does not show SLA propagation in the coastal region from the equator to the Bay of Bengal. Instead, positive SLAs appear to develop locally about 10 days prior, before rapidly increasing in the western coast of India. Previous studies proposed that intraseasonal SLA variations along the western coast of India are predominantly influenced by the propagation of the coastal Kelvin waves from the equatorial Indian Ocean (Suresh et al., 2013). Therefore, the results obtained in this study suggest that COCO-HR effectively captures the propagation of coastal Kelvin waves from the equator. However, the propagation of Kelvin waves from the equator is not well captured by COCO-LR due to the coarser horizontal resolution (Text S3), suggesting an exaggerated influence of local wind and/or thermal forcing in the western coast of India.

In the WIND0 composites, no SLA propagation originating from the equatorial Kelvin waves is evident. This is because the suppressed wind stress anomalies do not trigger intraseasonal anomalies of the equatorial Kelvin waves and, consequently, the coastal Kelvin waves in the Bay of Bengal. These results are also supported by the lag-composite analysis of SLA from 0 to 40 days following instances when the SLA exceeds +1 standard deviation at the eastern equatorial Indian Ocean (Fig. S7). While both COCO-HR and COCO-LR depict the propagation of equatorial Kelvin waves to the eastern boundary, only the observations and COCO-HR show the subsequent SLA propagation in the Bay of Bengal.

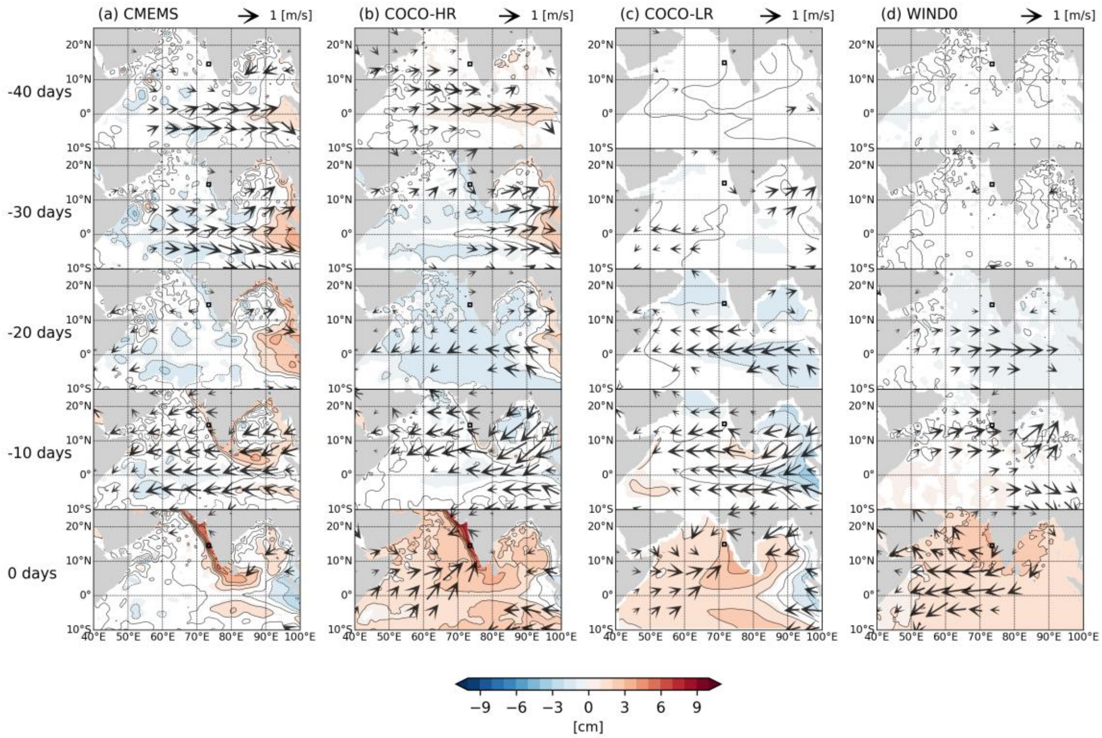

Figure 3. Lag-composites of sea level anomalies (SLA) (contour and color) and 10-m wind (vectors) for area-averaged SLA time series along the western coast of India (black boxes). Data are shown for (a) CMEMS, (b) COCO-HR, (c) COCO-LR, and (d) WIND0. Colors and vectors indicate statistically significant SLA and zonal wind anomalies at the 90% confidence level, respectively.

4.3 Influence of Indian Ocean Dipole on the probability distribution of coastal SLA along the western coast of India

In section 4.2, differences in PDFs of intraseasonal SLA are attributed to the representation of coastal Kelvin waves. This section examines the origin of the coastal Kelvin waves, particularly their association with wind variations in the tropical Indian Ocean. Given that basin-scale wind anomalies in the tropical Indian Ocean are affected by the IOD, it follows that the IOD contributes to interannual low-frequency SLA variations along the western coast of India through coastal Kelvin waves (e.g., Suresh et al., 2018). However, the extent to which interannual wind anomalies associated with the IOD modulate intraseasonal SLA variations, specifically the probability distribution of coastal SLA along the western coast of India, remains unclear. We therefore investigated the relationship between IOD and intraseasonal SLA, and assessed its representation in both COCO-HR and COCO-LR. In this analysis, the dipole mode index (DMI) is defined as the difference between area-averaged monthly-mean SST difference between the western (50°E-70°E, 10°S-10°N) and eastern (90°E-110°E, 10°S-0°) poles, as defined in previous studies (Saji et al., 1999; Tanizaki et al., 2017). A 3-month running mean is also applied to the DMI.

Since SST anomalies associated with the IOD typically peak in October (e.g., Saji et al., 1999), we focus on the relationship between the IOD and intraseasonal SLA along the western coast of India during this month. During positive IOD events, equatorial easterly wind anomalies trigger positive (negative) SLAs along the southern tip of Sri Lanka (in the eastern equatorial Indian Ocean) and, subsequently, positive (negative) coastal Kelvin waves along the western coast of India (coastal region of the Bay of Bengal) as observed (Fig. 4a). The SLAs associated with the IOD affects the interannual modulation of intraseasonal SLAs along the western coast of India (Fig. 4d). The correlation between the October-mean of intraseasonal SLAs and the DMI is 0.68, indicating that the IOD modulates the interannual variations in intraseasonal SLA. During the positive IOD phases, the PDF of the intraseasonal SLA shifts positively (Fig. 4g). Conversely, the PDFs during negative IOD and neutral years are less distinct, which may be attributed to the asymmetry in the IOD, with negative events having a smaller amplitude than positive events (e.g., Nakazato et al., 2021, An et al., 2023).

COCO-HR can simulate positive SLAs along the west Indian coast during the positive IOD (Fig. 4b). Also, the relatively strong correlation between intraseasonal SLA and DMI (r=0.48) are moderately represented (Fig. 4e), and the PDF shifts positively during positive IOD phases, as observed (Fig. 4h). On the other hand, although the SLA patterns along the west coast of India are similar during the IOD (Fig. 4a-c), intraseasonal SLAs are not correlated with the DMI (r=0.03) and the PDF does not shifts positively in COCO-LR (Fig. 4f, i).

While both COCO-HR and COCO-LR are driven by the same surface forcings, leading to similar large-scale SLA variation patterns in October, there are notable differences at a local scale. This discrepancy is particularly evident when focusing on the local SLA along the western coast of India, where COCO-LR fails to represent the interannual variations. Additionally, COCO-LR underestimates the variability in SLAs associated with intraseasonal variations, and the differences in PDFs between the IOD phases are not adequately represented (Fig. 4; Fig. S9). This issue in COCO-LR is likely due to its inability to adequately represent the propagation process of coastal waves originating from the equator, as discussed in the previous section. Therefore, we conclude that interannual wind anomalies associated with the IOD influence the occurrence of extreme SLAs along the western coast of India, and that this effect is represented in the eddy-resolving ocean model. Furthermore, while the non-eddying model can represent the low-frequency SLA patterns associated with the IOD, it lacks the necessary resolution to simulate modulations in extreme intraseasonal SLAs.

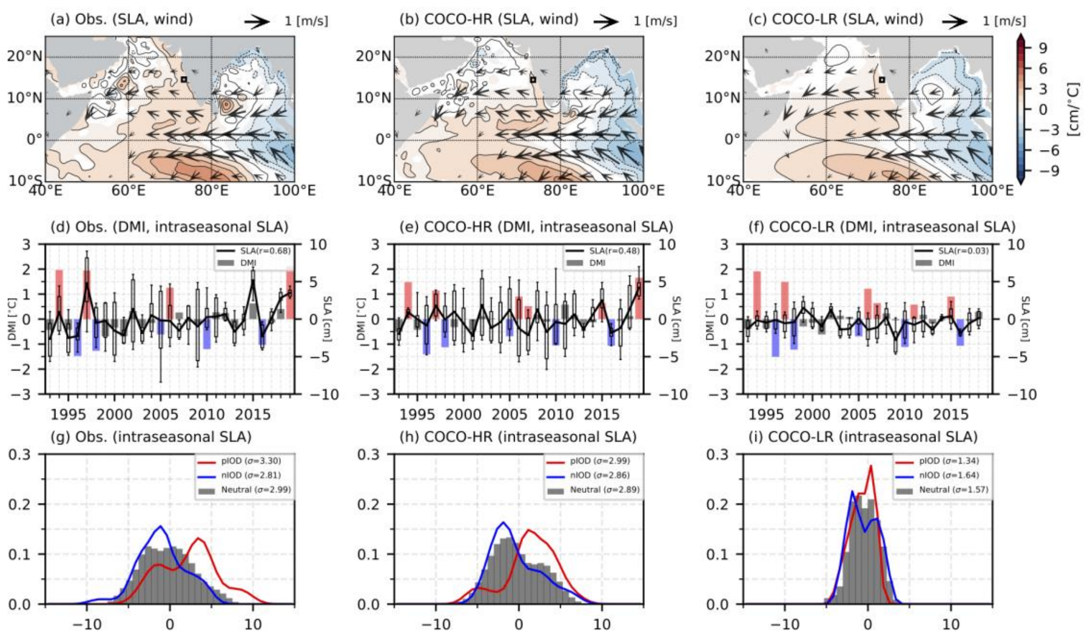

Figure 4. (a) Regressions of October-mean sea level anomalies (SLAs) and 10 m wind anomalies to September-October-November (SON)-mean dipole mode index (DMI) for CMEMS and JRA55-do data. Colors and vectors indicate statistically significant regression coefficients for SLAs and zonal winds at the 90% confidence level, respectively. (d) Time series of the DMI (bar) and intraseasonal SLA (i.e., bandpassed for 20-150 days) (line) during October along the western Indian coast (15°N; black box in (a)), based on observational data. The correlation between DMI and October-mean intraseasonal SLA is shown in the legend of each graph. Red (blue) bars indicate positive (negative) IOD, while gray bars indicate neutral years. Daily intraseasonal SLAs for a 31-day period, October, are depicted using box-whisker plots, where boxes span the 25% to 75% ranges in the data, the line indicates the monthly mean, and the

whiskers indicate the 5% to 95% ranges in the data. (g) PDFs for intraseasonal SLAs based on observational data for October, as in Fig. 2, but for during positive IOD years (red line), negative IOD years (blue line), and neutral years (gray bars). (b),(e),(h) As in (a), (d), (g), but for COCO-HR. (c),(f),(i) As in (a),(d),(g), but for COCO-LR.

5 Summary and discussion

This study showed that only the eddy-resolving OGCM (COCO-HR) is capable of reproducing the intraseasonal variability of SLAs along the western coast of India. The results indicate that COCO-HR effectively represents extreme SLA events along the western coast of India. Conversely, the non-eddying model (COCO-LR) fails to capture more than 81% of these extreme intraseasonal sea level events. In the COCO-HR model, equatorial Kelvin waves originating in the equatorial ocean enter the eastern boundary and subsequently propagate along the coast of the Bay of Bengal and western India, while COCO-LR fails it due to the coarser horizontal resolution. Furthermore, changes in the PDFs of intraseasonal SLAs associated with the IOD are captured only in the COCO-HR model. This suggests that basin-scale wind anomalies in the equatorial Indian Ocean can modulate the occurrence of extreme SLA events along the western coast of India.

The underestimation of coastal extreme sea level events in the non-eddying OGCM further implies that such extremes may be underestimated in CMIP6 models. In the context of recent research on extreme weather events and their links to a warming climate, several studies have emphasized the large-scale drivers of local extreme events (Kawase et al., 2019; Imada et al., 2020). Our results show that the probability of local sea level extremes along the western coast of India is also affected by large-scale wind anomalies associated with the IOD, thus demonstrating a "global-to-local" approach in oceanic cntexts. While this study focused on the IOD, future studies should examine the impacts of intraseasonal atmospheric variability, such as the MJO and the Boreal Summer Intraseasonal Oscillation (Wang & Xie, 1997) on coastal SLAs. Consequently, a reassessment of the risk of extreme sea level events, such as storm surges and floods in the coastal areas of the North Indian Ocean, may be needed. This reassessment should focus on the resolution of ocean models to better understand the relationship between changes in local coastal sea level extremes and basin-scale climate variability under global warming.

Acknowledgments

This work was supported by the MEXT program for advanced studies of climate change projection (SENTAN) (Grant Number JPMXD0722680395), and also by a joint research program between the Ministry of Earth Sciences (MoES) in India and JAMSTEC on ocean downscaling of climate model projections in Indian coastal regions to assess the coastal impact of sea level rise under conditions of global warming. The first author was supported by JSPS KAKENHI Grant Numbers JP20H05729, JP22K14098, and JP22H04487.

Open Research

The altimeter products were produced and distributed by Copernicus Marine Environment Monitoring Service (https://doi.org/10.48670/moi-00148). Drifter-derived data was downloaded from https://www.aoml.noaa.gov/ftp/phod/pub/lumpkin/drifter_climatology/. JRA55-do data (https://esgf-node.llnl.gov/search/input4mips), PCMDI-SST (https://aims2.llnl.gov/search/input4mips/?institution_id=PCMDI&source_version=1.1.9), and COCO-LR outputs (http://esgf-node.llnl.gov/search/cmip6/?mip_era=CMIP6&activity_id=OMIP&institution_id=MIROC&source_id=MIROC6&experiment_id=omip2) are now distributed through the Earth System Grid Federation. The COCO-HR and WIND0 data have been deposited in the Zenodo (https://doi.org/10.5281/zenodo.10633562).

References

1. An, S. I., Park, H. J., Kim, S. K., Cai, W., Santoso, A., Kim, D., & Kug, J. S. (2023). Main drivers of Indian Ocean Dipole asymmetry revealed by a simple IOD model. *npj Climate and Atmospheric Science*, *6*(1), 93. https://doi.org/10.1038/s41612-023-00422-2
2. Aparna, S. G., McCreary, J. P., Shankar, D., & Vinayachandran, P. N. (2012). Signatures of Indian Ocean Dipole and El Niño–Southern Oscillation events in sea level variations in the Bay of Bengal. *Journal of Geophysical Research*, 117, C10012. https://doi.org/10.1029/2012JC008055
3. Chelton, D. B., deSzoeke, R. A., Schlax, M. G., Naggar, K. E., & Siwertz, N. (1998).

Geographical variability of the first baroclinic Rossby radius of deformation. *Journal of Physical Oceanography*, *28*, 433–460, https://doi.org/10.1175/1520-0485(1998)028,0433:GVOTFB.2.0.CO;2.

4. Clarke, A. J., & Liu, X. (1994). Interannual sea level in the northern and eastern Indian Ocean. *Journal of Physical Oceanography*, *24*(6), 1224-1235.
5. Dehnad, K. (1987). Density estimation for statistics and data analysis. Technometrics, 29:4, 495, https://doi.org/10.1080/00401706.1987.10488295
6. Gill, A. E. (1982). *Atmosphere-ocean dynamics.* New York: Academic Press.
7. Gordon, A. L., Sprintall, J., Van Aken, H. M., Susanto, D., Wijffels, S., Molcard, R., et al. (2010). The Indonesian throughflow during 2004–2006 as observed by the INSTANT program. *Dynamics of Atmospheres and Oceans*, 50(2), 115-128. https://doi.org/10.1016/j.dynatmoce.2009.12.002.
8. Han, W., & Webster, P. J. (2002). Forcing mechanisms of sea level interannual variability in the Bay of Bengal. *Journal of Physical Oceanography*, 32(1), 216-239. https://doi.org/10.1175/1520-0485(2002)032<0216:FMOSLI>2.0.CO;2
9. Han, W., Meehl, G. A., Rajagopalan, B., Fasullo, J. T., Hu, A., Lin, J., et al. (2010). Patterns of Indian Ocean sea-level change in a warming climate. *Nature Geoscience*, 3(8), 546-550. https://doi.org/10.1038/ngeo901
10. Han, W., McCreary, J. P., Masumoto, Y., Vialard, J., & Duncan, B. (2011). Basin resonances in the equatorial Indian Ocean. *Journal of Physical Oceanography*, 41(6), 1252-1270. https://doi.org/10.1175/2011JPO4591.1
11. Hasumi, H., 2006: CCSR Ocean Component Model (COCO) version 4.0. *CCSR Technical Report*, 25, 103 pp., https://ccsr.aori.utokyo.ac.jp/;hasumi/COCO/coco4.pdf.
12. Hurrell, J. W., Hack, J. J., Shea, D., Caron, J. M., & Rosinski, J. (2008). A new sea surface temperature and sea ice boundary dataset for the Community Atmosphere Model. *Journal of Climate*, *21*(19), 5145-5153. https://doi.org/10.1175/2008JCLI2292.1
13. Imada, Y., Kawase, H., Watanabe, M., Arai, M., Shiogama, H., & Takayabu, I. (2020). Advanced risk-based event attribution for heavy regional rainfall events. *npj climate and atmospheric science*, *3*(1), 37. https://doi.org/10.1038/s41612-020-00141-y
14. Intergovernmental Panel on Climate Change (IPCC). (2022a). Sea Level Rise and Implications for Low-Lying Islands, Coasts and Communities. In *The Ocean and*

Cryosphere in a Changing Climate: Special Report of the Intergovernmental Panel on Climate Change (pp. 321–446). chapter, Cambridge: Cambridge University Press. https://doi.org/10.1017/9781009157964.006

15. Intergovernmental Panel on Climate Change (IPCC). (2022b). Extremes, Abrupt Changes and Managing Risks. In *The Ocean and Cryosphere in a Changing Climate: Special Report of the Intergovernmental Panel on Climate Change* (pp. 589–656). Cambridge: Cambridge University Press. https://doi.org/10.1017/9781009157964.008.
16. Jyoti, J., Swapna, P., & Krishnan, R. (2023). North Indian Ocean sea level rise in the past and future: The role of climate change and variability. *Global and Planetary Change*, 228, 104205. https://doi.org/10.1016/j.gloplacha.2023.104205
17. Kawase, H., Imada, Y., Sasaki, H., Nakaegawa, T., Murata, A., Nosaka, M., & Takayabu, I. (2019). Contribution of historical global warming to local-scale heavy precipitation in western Japan estimated by large ensemble high-resolution simulations. *Journal of Geophysical Research: Atmospheres*, *124*(12), 6093-6103. https://doi.org/10.1029/2018JD030155
18. Komuro, Y. (2019). *MIROC MIROC6 model output prepared for CMIP6 OMIP omip2*. Version *YYYYMMDD*. Earth System Grid Federation. https://doi.org/10.22033/ESGF/CMIP6.5655
19. Laurindo, L. C., Mariano, A. J., & Lumpkin, R. (2017). An improved near-surface velocity climatology for the global ocean from drifter observations. *Deep Sea Research Part I: Oceanographic Research Papers*, *124*, 73-92. https://doi.org/10.1016/j.dsr.2017.04.009
20. Locarnini, M. M., Mishonov, A. V., Baranova, O. K., Boyer, T. P., Zweng, M. M., Garcia, H. E., et al. (2018). World ocean atlas 2018, volume 1: Temperature. NOAA Atlas NESDIS 81, 52pp. https://archimer.ifremer.fr/doc/00651/76338/
21. Madden, R. A., & Julian, P. R. (1971). Detection of a 40–50 day oscillation in the zonal wind in the tropical Pacific. *Journal of Atmospheric Sciences*, 28(5), 702-708. https://doi.org/10.1175/1520-0469(1971)028%3C0702:DOADOI%3E2.0.CO;2
22. Marshall, J., & Molteni, F. (1993). Toward a dynamical understanding of planetary-scale flow regimes. *Journal of the Atmospheric Sciences*, 50(12), 1792-1818. https://doi.org/10.1175/1520-0469(1993)050%3C1792:TADUOP%3E2.0.CO;2

23. McCreary Jr, J. P., Kundu, P. K., & Molinari, R. L. (1993). A numerical investigation of dynamics, thermodynamics and mixed-layer processes in the Indian Ocean. *Progress in Oceanography*, *31*(3), 181-244. https://doi.org/10.1016/0079-6611(93)90002-U
24. Nakano, H., & Suginohara, N. (2002). Effects of bottom boundary layer parameterization on reproducing deep and bottom waters in a world ocean model. *Journal of Physical Oceanography*, *32*(4), 1209-1227. https://doi.org/10.1175/1520-0485(2002)032%3C1209:EOBBLP%3E2.0.CO;2
25. Nakazato, M., Kido, S., & Tozuka, T. (2021). Mechanisms of asymmetry in sea surface temperature anomalies associated with the Indian Ocean Dipole revealed by closed heat budget. *Scientific Reports*, *11*(1), 22546. https://doi.org/10.1038/s41598-021-01619-2
26. Pujol, M. I., Faugère, Y., Taburet, G., Dupuy, S., Pelloquin, C., Ablain, M., & Picot, N. (2016). DUACS DT2014: the new multi-mission altimeter data set reprocessed over 20 years. *Ocean Science*, *12*(5), 1067-1090. https://doi.org/10.5194/os-12-1067-2016.
27. Ridderinkhof, H., Van der Werf, P. M., Ullgren, J. E., Van Aken, H. M., Van Leeuwen, P. J., & de Ruijter, W. P. M. (2010). Seasonal and interannual variability in the Mozambique Channel from moored current observations. *Journal of Geophysical Research: Oceans*, *115*(C6). https://doi.org/10.1029/2009JC005619
28. Saji, N. H., Goswami, B. N., Vinayachandran, P. N., & Yamagata, T. (1999). A dipole mode in the tropical Indian Ocean. *Nature*, *401*(6751), 360-363. https://doi.org/10.1038/43854
29. Suresh, I., Vialard, J., Lengaigne, M., Han, W., McCreary, J., Durand, F., & Muraleedharan, P. M. (2013). Origins of wind-driven intraseasonal sea level variations in the North Indian Ocean coastal waveguide. *Geophysical Research Letters*, *40*(21), 5740-5744. https://doi.org/10.1002/2013GL058312
30. Suresh, I., Vialard, J., Izumo, T., Lengaigne, M., Han, W., McCreary, J., & Muraleedharan, P. M. (2016). Dominant role of winds near Sri Lanka in driving seasonal sea level variations along the west coast of India. *Geophysical Research Letters*, *43*(13), 7028-7035. https://doi.org/10.1002/2016GL069976.
31. Suresh, I., Vialard, J., Lengaigne, M., Izumo, T., Parvathi, V., & Muraleedharan, P. M. (2018). Sea level interannual variability along the west coast of India. *Geophysical Research Letters*, *45*(22), 12-440. https://doi.org/10.1029/2018GL080972
32. Tanizaki, C., Tozuka, T., Doi, T., & Yamagata, T. (2017). Relative importance of the

processes contributing to the development of SST anomalies in the eastern pole of the Indian Ocean Dipole and its implication for predictability. *Climate Dynamics*, *49*, 1289-1304. https://doi.org/10.1007/s00382-016-3382-2

33. Tatebe, H., Ogura, T., Nitta, T., Komuro, Y., Ogochi, K., Takemura, T., et al. (2019). Description and basic evaluation of simulated mean state, internal variability, and climate sensitivity in MIROC6. *Geoscientific Model Development*, *12*(7), 2727-2765. https://doi.org/10.5194/gmd-12-2727-2019
34. Tsujino, H., Urakawa, L. S., Griffies, S. M., Danabasoglu, G., Adcroft, A. J., Amaral, A. E., et al. (2020). Evaluation of global ocean–sea-ice model simulations based on the experimental protocols of the Ocean Model Intercomparison Project phase 2 (OMIP-2). *Geoscientific Model Development*, *13*(8), 3643-3708. https://doi.org/10.5194/gmd-13-3643-2020
35. Varna, M., Jithin, A. K., & Francis, P. A. (2023). Characteristics and dynamics of mesoscale eddies in the eastern Arabian Sea. *Deep Sea Research Part II: Topical Studies in Oceanography*, *207*, 105218. https://doi.org/10.1016/j.dsr2.2022.105218
36. Vinayachandran, P. N., Shankar, D., Kurian, J., Durand, F., & Shenoi, S. S. C. (2007). Arabian Sea mini warm pool and the monsoon onset vortex. *Current Science*, *93*(2), 203–214. http://www.jstor.org/stable/24099306
37. Wang, B., & Xie, X. (1997). A model for the boreal summer intraseasonal oscillation. *Journal of the Atmospheric Sciences*, *54*(1), 72-86. https://doi.org/10.1175/1520-0469(1997)054%3C0072:AMFTBS%3E2.0.CO;2
38. Wyrtki, K. (1973). An equatorial jet in the Indian Ocean. *Science*, *181*(4096), 262-264. https://doi.org/10.1126/science.181.4096.262
39. Yoshida, K. (1960). A Theory of the Cromwell Current (the Equatorial Undercurrent) and of the Equatorial Upwelling. *Journal of the Oceanographical Society of Japan*, *15*(4), 159-170. https://doi.org/10.5928/kaiyou1942.15.159
40. Zweng, M. M., Seidov, D., Boyer, T. P., Locarnini, M., Garcia, H. E., Mishonov, A. V., et al. (2019). World ocean atlas 2018, volume 2: Salinity. NOAA Atlas NESDIS 82, 50pp. https://archimer.ifremer.fr/doc/00651/76339/

Geophysical Research Letters

Supporting Information for

Intraseasonal sea level variability along the western coast of India in an eddy-resolving ocean general circulation model

Y. Yamagami[1], T. Suzuki[1], and H. Tatebe[1]

[1] Japan Agency for Marine-Earth Science and Technology, Yokohama, Japan

Contents of this file

Text S1 to S3

Figures S1 to S9

Introduction

This document contains supplementary documents and figures referred to in the main article.

Text S1

Model validation

We provide a brief validation of the COCO-HR model. When compared to observational data, COCO-HR simulations effectively reproduce the mean thermal and mechanical fields in the Indian Ocean. Model biases in SST are reduced in COCO-HR (Fig. S1). The model also realistically simulates key features of the mean circulation in the Indian Ocean, such as Indonesian Throughflow (12.2 ± 2.9 Sv compared to about 13 Sv in observations; Gordon et al., 2010) and the Mozambique Channel flow (16.3 ± 5.6 Sv compared to about 16.7 ± 8.9 Sv in observations; Ridderinkhof et al., 2010). In addition, tropical equatorial stratification is also realistically reproduced in COCO-HR, showing slight improvements compared to COCO-LR (Fig. S2). The seasonal cycle in the tropical Indian Ocean, which is characterized by semiannual surface velocity variations known as the Wyrtki jet (Yoshida, 1959; Wyrtki, 1973), was also reproduced in both COCO-HR and COCO-LR (Fig. S3). The zonal surface velocities in both models are smaller compared to those derived from drifters, with COCO-HR exhibiting a slight improvement in this bias. This result suggests that the basin-wide resonance between forced and reflected equatorial waves might be captured in these models (Han et al., 2011).

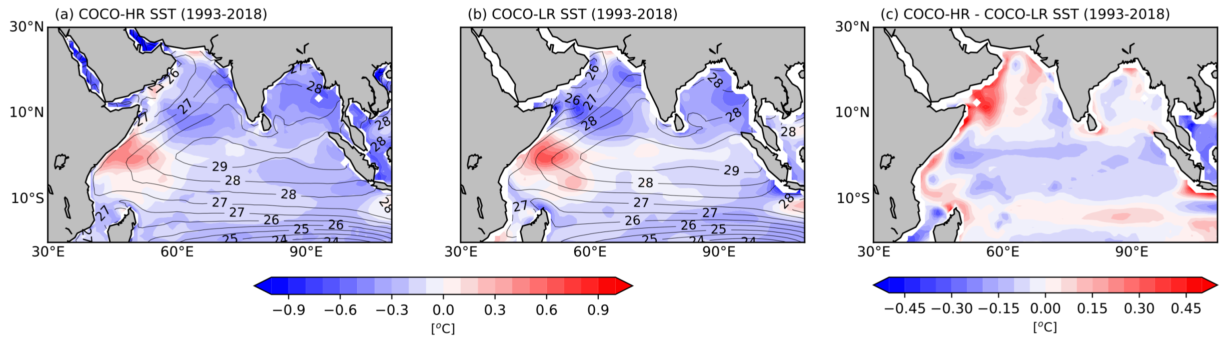

Figure S1. Sea surface temperature (SST) biases compared to PCMDI-SST for (a) COCO-HR and (b) COCO-LR for the period 1993-2018. Contours indicate the climatology in the models. (c) Difference in SST between COCO-HR and COCO-LR.

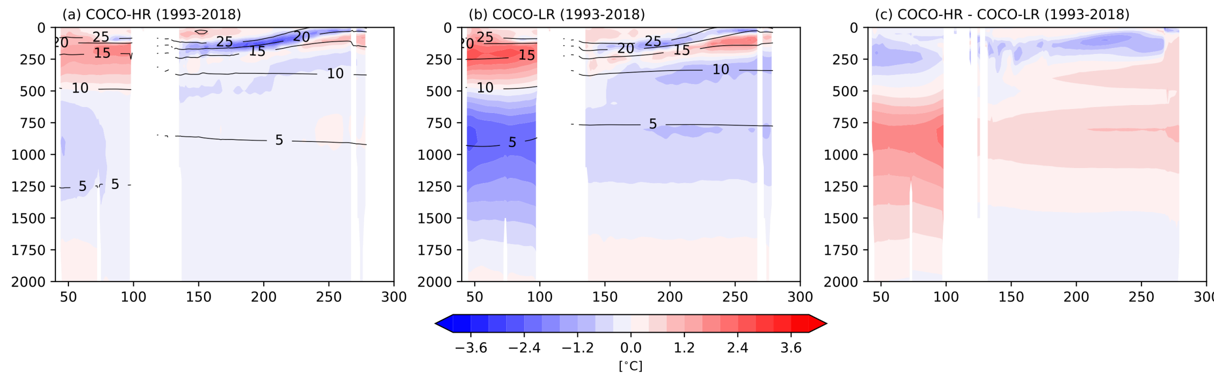

Figure S2. Temperature biases to WOA13v2 along the equator for (a) COCO-HR and (b) COCO-LR during the period 1993-2018 in the Indo-Pacific Ocean. The vertical axis represents depth [m] and contours indicate the climatology in the models. (c) Difference in temperature between COCO-HR and COCO-LR.

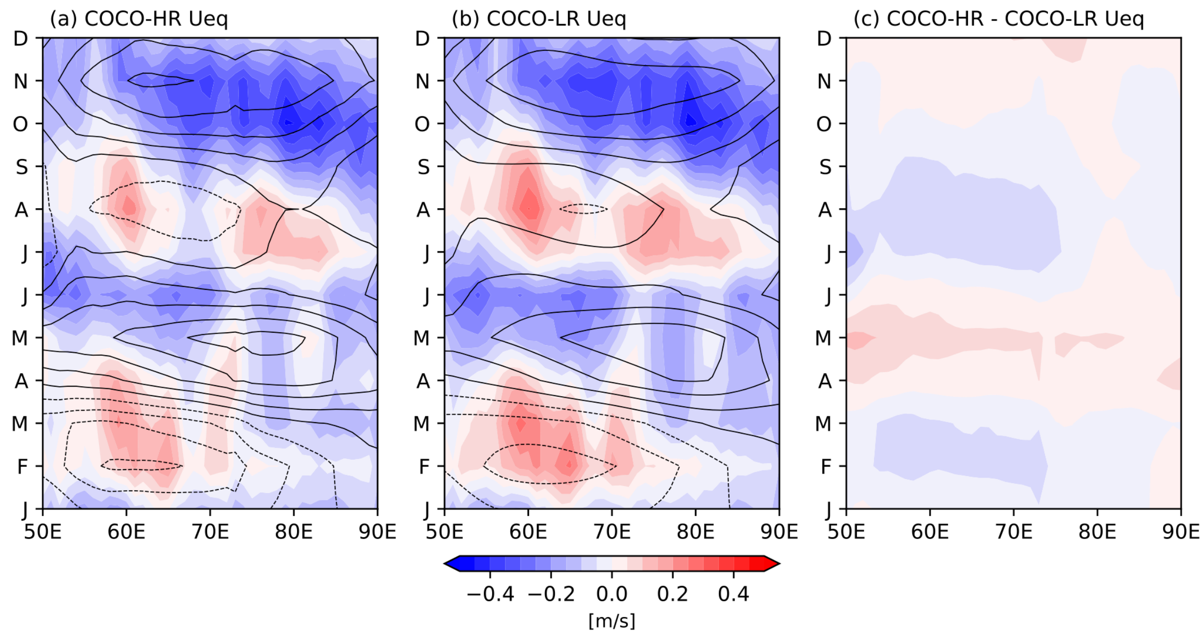

Figure S3. Zonal surface velocity bias along the equator (2.5°S-2.5°N) to the drifter-derived observation (Laurindo et al., 2017) for (a) COCO-HR and (b) COCO-LR during the period 1993-2018. Shaded areas show the difference from observations, and contours indicate the climatology for each model with 0.1 m/s intervals. The vertical axis indicates the seasonal progression, while the horizontal axis indicates longitude. (c) As in (a), but for the difference between COCO-HR and COCO-LR.

Text S2

Seasonal variations in SLAs for COCO-HR and COCO-LR

According to observations, the seasonal variations peak during winter (January) and reach their lowest in summer (August) (Fig. S4). The seasonal variations in COCO-HR closely align with the observations, with slight differences in the timing of the minimum. On the other hand, COCO-LR shows that the peak maximum occurs in April, and significantly underestimates the amplitude during winter, suggesting a lack of the key physical processes that explain these seasonal variations. Since the seasonal SLA variations are primarily driven by wind forcing over the southern tip of Sri Lanka, the Bay of Bengal, and the equator (Suresh et al., 2016), these results imply that COCO-LR may underestimate the adjustments by coastal Kelvin waves along the western coast of India.

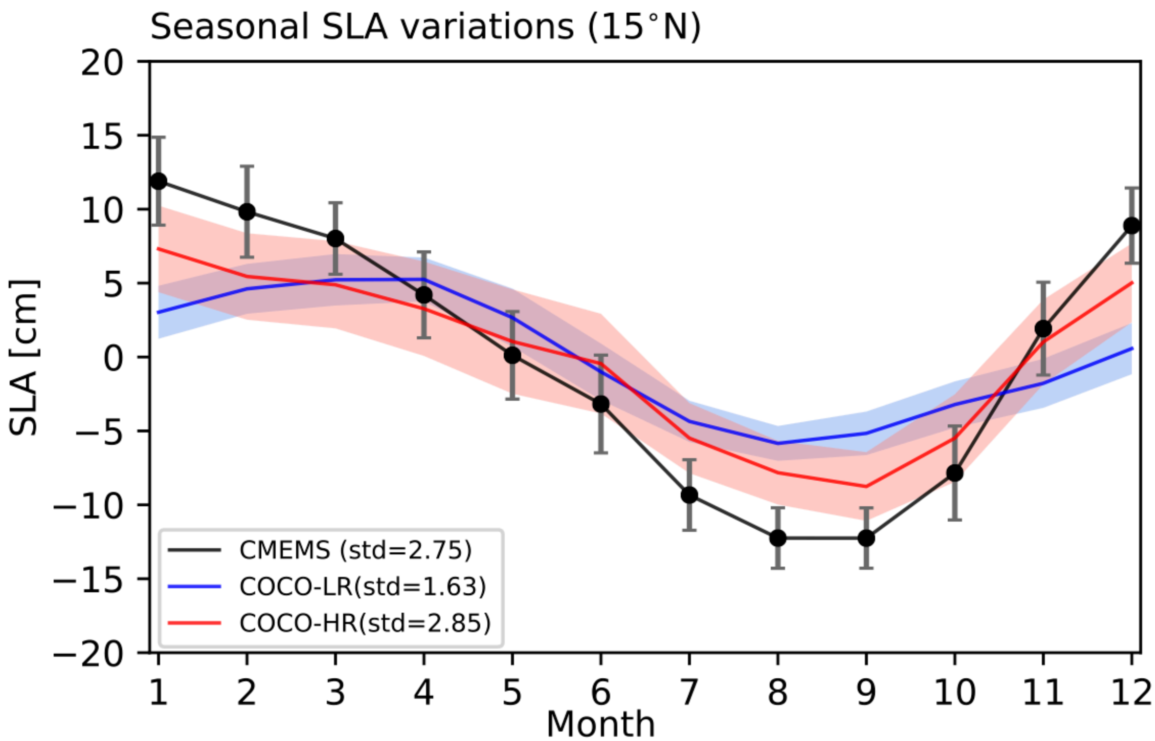

Figure S4. Seasonal variations in SLAs [cm] along the western coast of India (15°N; black boxes in Fig. 1) for the observations (CMEMS; black line), COCO-LR (blue line), and COCO-HR (red line). Bars and shaded areas indicate ±1 standard deviation. The annual mean has been subtracted from each time series to highlight the seasonal variations.

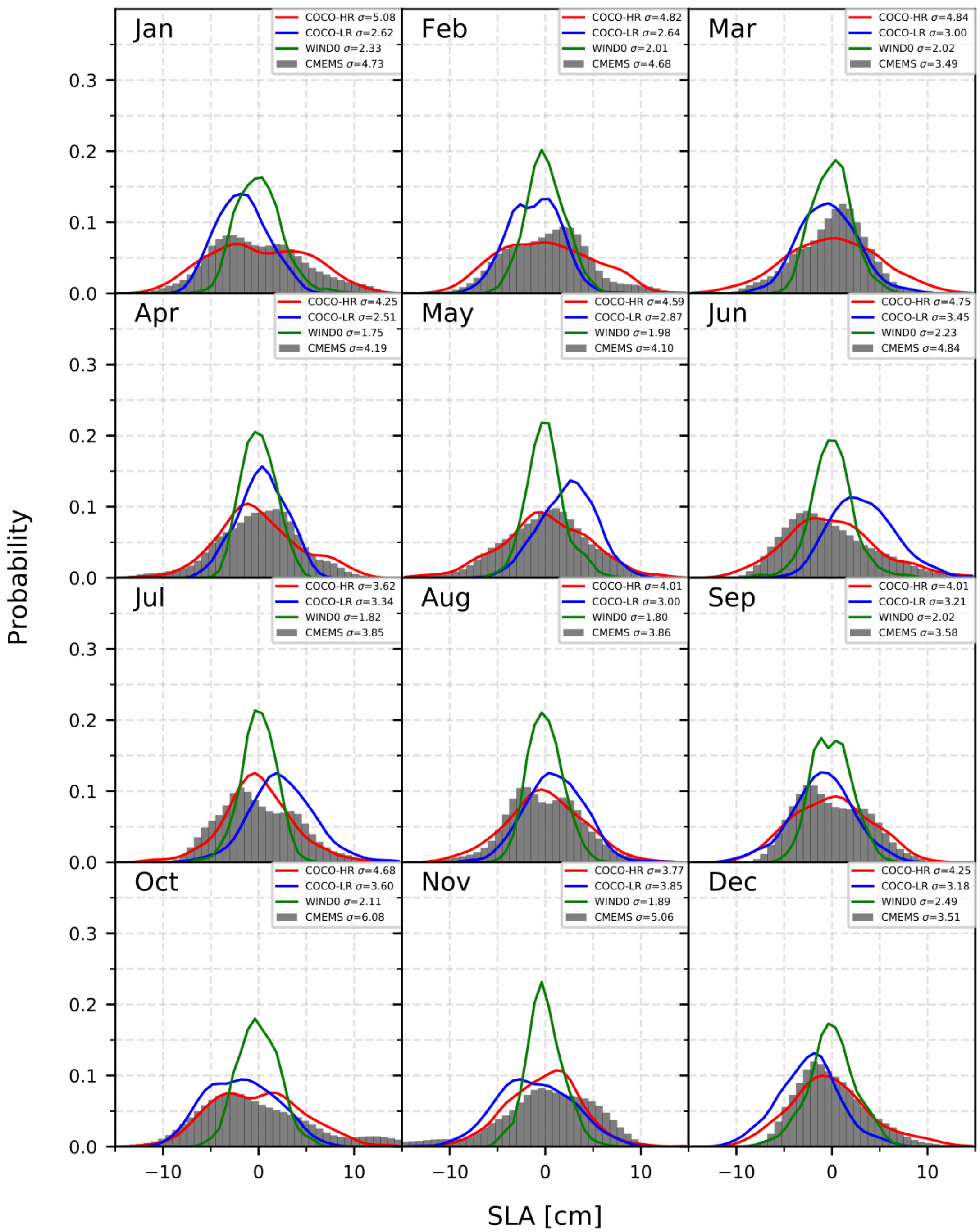

Figure S5. As in Figure 2, but for detrended SLAs without applying a bandpass filter.

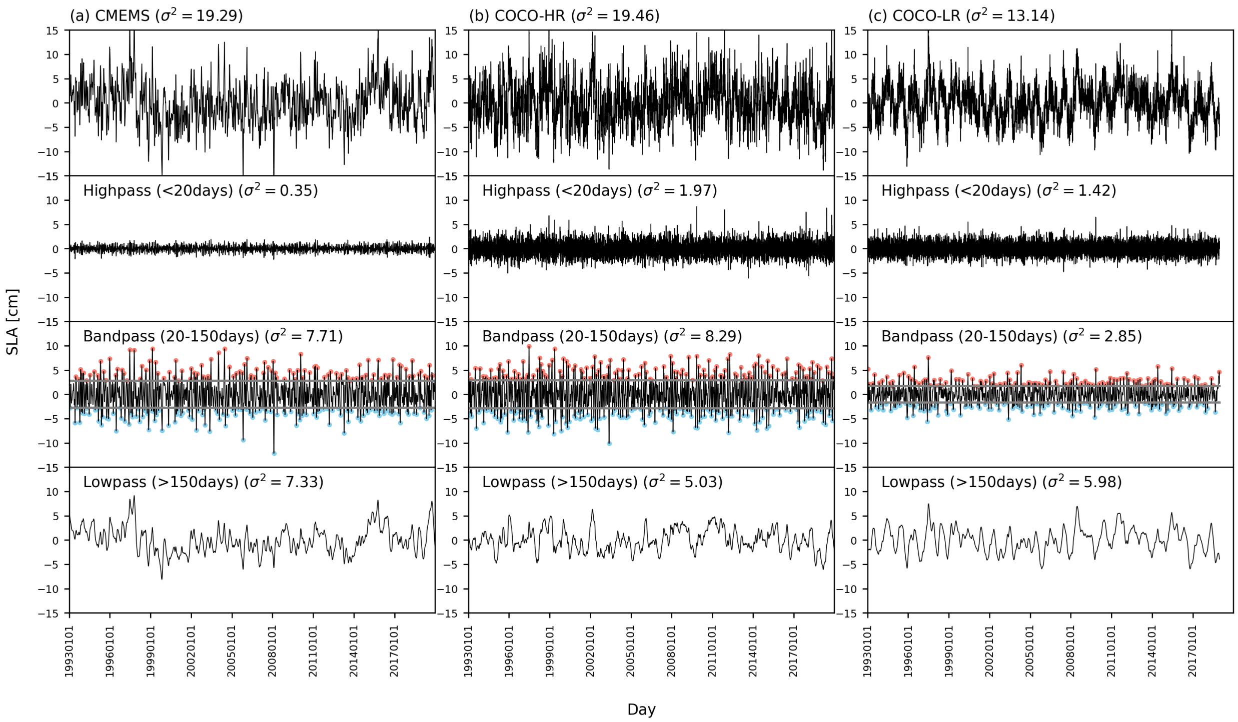

Figure S6. Variations in SLAs [cm] along the western coast of India (15°N; black boxes in Fig. 1) for (a) observations (CMEMS), (b) COCO-HR (blue line), and (c) COCO-LR. Top panels show detrended daily anomalies, while lower panels show the time series filtered into three frequency bands: high-pass (shorter than 20 days), band-pass (20-150 days), and low-pass (longer than 150 days). The variance for timeseries is shown in each panel.

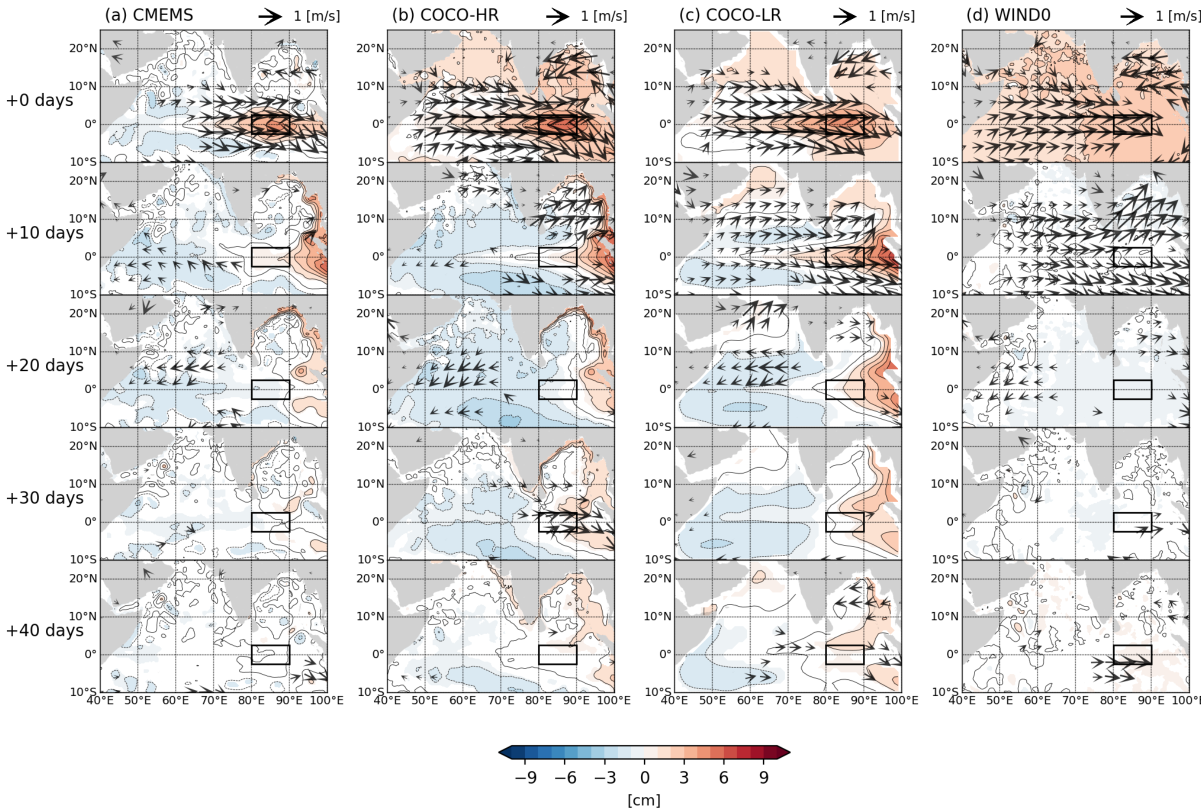

Figure S7. As in Figure 3, but for lag-composites for area-averaged SLA timeseries in the equatorial Indian Ocean (80°-90°E, 5°S-5°N; black boxes).

Text S3

Sufficient resolution for simulating coastal Kelvin waves

In this section, to examine the resolution dependency on representing coastal Kelvin waves, the model horizontal resolution is compared to the simulated Rossby deformation radius. Internal coastal Kelvin waves have a typical spatial scale of the Rossby deformation radius (e.g., Gill, 1982). The phase speed (c_1) and deformation radius (λ_1) of the first mode of the baroclinic Rossby wave, under the WKB approximation, are defined as follows (Chelton et al., 1998):

$$c_1 \approx \frac{1}{\pi}\int_{-H}^{0} N(z)\,dz \quad (1),$$

$$\lambda_1 = \begin{cases} \dfrac{c_1}{|f(\vartheta)|} & if\ |\vartheta| \geq 5° \\ \left(\dfrac{c_1}{2\beta(\vartheta)}\right)^{1/2} & if\ |\vartheta| < 5° \end{cases} \quad (2).$$

Where H is the depth of the ocean, $N(z)$ is the buoyancy frequency, ϑ is latitude, $f(\vartheta)$ is the Coriolis parameter, and $\beta(\vartheta)$ is the meridional gradient of $f(\vartheta)$. Figure S8 shows the estimated deformation radius for both COCO-HR and COCO-LR models. Both models have similar c_1 throughout the North Indian Ocean because of the similar stratification structure. However, since only COCO-HR can resolve continental shelves and steep ridges, the values differ around the atolls of the Maldives, in coastal areas of the Bay of Bengal, and along the western coast of India.

When comparing the nominal resolution of COCO-HR (COCO-LR), defined as $\Delta x = 0.1°\ (1.0°)$, with the deformation radius, there is a significant difference between the two. In COCO-HR, the resolution is sufficient (i.e., $\lambda_1 > 2\Delta x$) throughout the North Indian Ocean, except over the shallow continental shelf region, suggesting that COCO-HR is sufficient to represent coastal Kelvin waves. However, COCO-LR satisfies $\lambda_1 > 2\Delta x$ only in the equatorial regions, suggesting that the model lacks sufficient resolution in the North Indian Ocean.

We note that the comparison between deformation radius and resolution provides only a rough estimate. This is because rapid variations in $N(z)$ due to mixed layers in the upper ocean can introduce errors in the estimation of c_1 under the WKB approximation (Chelton et al., 1998). It is also important to note that SLA propagation from the equator may be transformed into continental shelf waves, and local dynamics such as local coastal winds, instability, and river runoff can interrupt this propagation. However, previous studies have shown that coastal Kelvin waves are a key factor in explaining SLA variations along the western coast of India (e.g., Suresh et al., 2013). This suggests that the ability of COCO-HR to resolve coastal Kelvin waves contributes significantly to its reasonable representation of extreme SLA variations in this region.

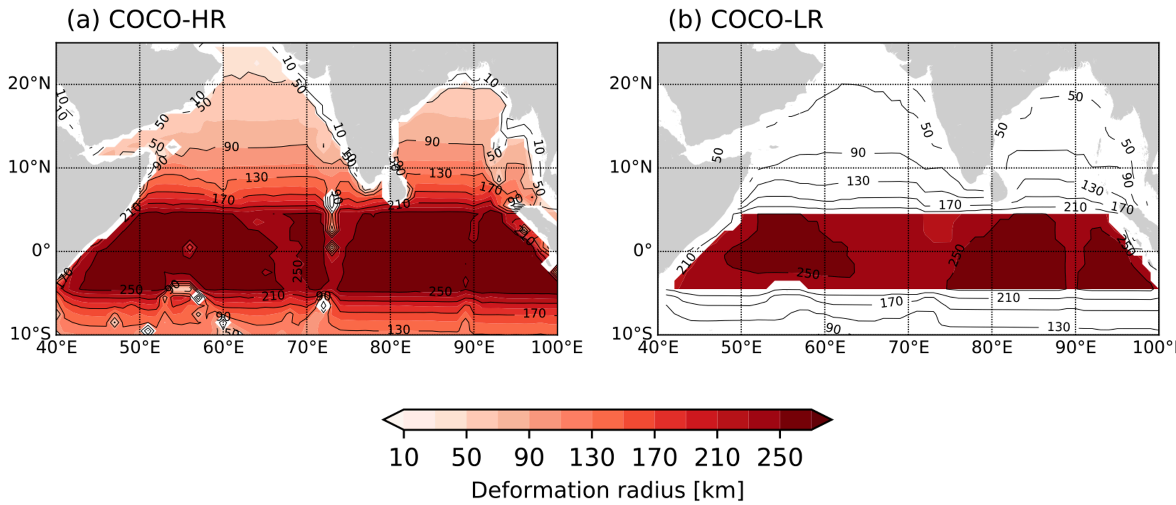

Figure S8. Deformation radius (λ_1) of the first mode of the baroclinic Rossby wave (Eq. 2) for (a) COCO-HR and (b) COCO-LR. The color indicates the area where the nominal horizontal resolution (Δx) is finer than the deformation radius (i.e., $\lambda_1 > 2\Delta x$).

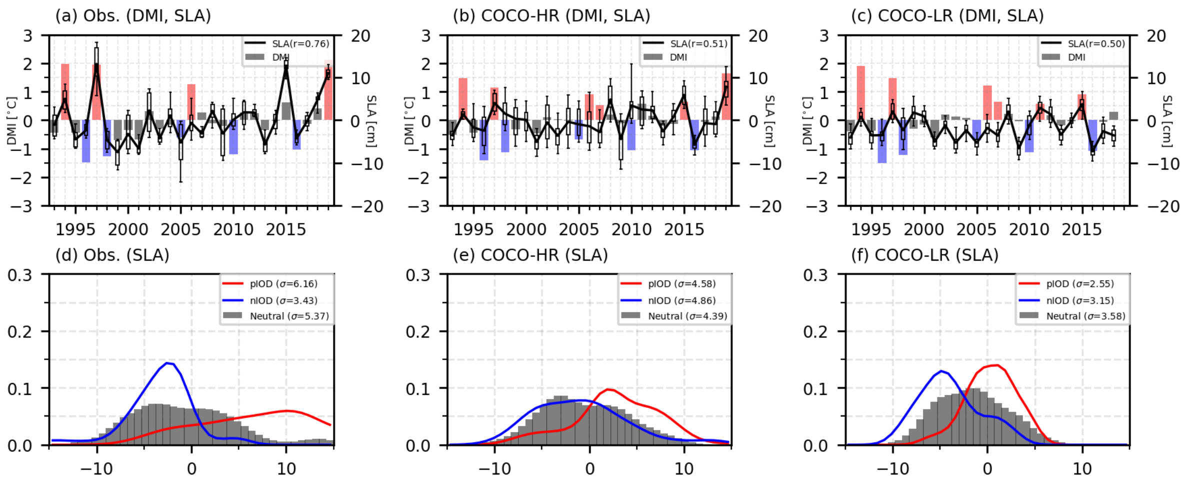

Figure S9. As for Figure 4, but for SLA timeseries without applying a bandpass filter.